Therapeutic antibody targeting of Notch3 signaling prevents mural cell loss in CADASIL

Arturo I. Machuca-Parra,[1]* Alexander A. Bigger-Allen,[1]* Angie V. Sanchez,[1] Anissa Boutabla,[1,3] Jonathan Cardona-Vélez,[1,4] Dhanesh Amarnani,[1] Magali Saint-Geniez,[1] Christian W. Siebel,[5] Leo A. Kim,[1] Patricia A. D'Amore,[1,2] and Joseph F. Arboleda-Velasquez[1]

[1]Schepens Eye Research Institute of Massachusetts Eye and Ear, Department of Ophthalmology and [2]Department of Pathology, Harvard Medical School, Boston, MA
[3]Grenoble Alpes University, Grenoble, France
[4]Universidad Pontificia Bolivariana, Medellín, Colombia
[5]Department of Discovery Oncology, Genentech, Inc., South San Francisco, CA

Cerebral autosomal-dominant arteriopathy with subcortical infarcts and leukoencephalopathy (CADASIL) is a neurological syndrome characterized by small vessel disease (SVD), stroke, and vascular cognitive impairment and dementia caused by mutations in *NOTCH3*. No therapies are available for this condition. Loss of mural cells, which encompass pericytes and vascular smooth muscle cells, is a hallmark of CADASIL and other SVDs, including diabetic retinopathy, resulting in vascular instability. Here, we showed that Notch3 signaling is both necessary and sufficient to support mural cell coverage in arteries using genetic rescue in Notch3 knockout mice. Furthermore, we show that systemic administration of an agonist Notch3 antibody prevents mural cell loss and modifies plasma proteins associated with Notch3 activity, including endostatin/collagen 18α1 and Notch3 extracellular domain in mice with the C455R mutation, a CADASIL variant associated with Notch3 loss of function. These findings open opportunities for the treatment of CADASIL and other SVDs by modulating Notch3 signaling.

The Journal of Experimental Medicine

INTRODUCTION

Mutations in *NOTCH3*, leading to a Notch3 receptor with unpaired cysteines in the epidermal growth factor–like repeats (EGF-like) are the cause of cerebral autosomal-dominant arteriopathy with subcortical infarcts and leukoencephalopathy (CADASIL), the most common monogenic cause of cerebral small vessel disease (SVD; Joutel et al., 1996; Chabriat et al., 2009). Recent analyses of public exome databases found a prevalence of 3.4/1,000 for CADASIL mutations (Rutten et al., 2016). It has been proposed that CADASIL mutations trigger aggregation of the Notch3 extracellular domain and aberrant interactions between it and other proteins, leading to neomorphic effects (Arboleda-Velasquez et al., 2005; Chabriat et al., 2009; Joutel et al., 2016). CADASIL mutations located in the ligand-binding domain of the Notch3 receptor and those that impair plasma membrane localization overtly impair Notch3 downstream signaling (Arboleda-Velasquez et al., 2002, 2011; Joutel et al., 2004). A distinct class of *NOTCH3* mutations, including premature stop codons or frame-shift mutations in *NOTCH3*, are also associated with cerebral SVD, stroke, and vascular cognitive impairment and dementia; patients with these loss-of-function mutations in *Notch3* develop symptoms later in life, show incomplete penetrance, and lack CADASIL's characteristic vascular deposits (e.g., Notch3 extracellular domain and granular osmiophilic material; Dotti et al., 2004; Rutten et al., 2013; Erro et al., 2015; Moccia et al., 2015; Pippucci et al., 2015; Yoon et al., 2015). Consistent with the pathobiology of these human conditions, CADASIL and Notch3 knockout mice develop mural cell loss and dysfunction (Arboleda-Velasquez et al., 2011; Ghosh et al., 2015; Henshall et al., 2015; Kofler et al., 2015; Baron-Menguy et al., 2017).

In mammalian cells, Notch receptors at the plasma membrane are heterodimers resulting from an S1 proteolytic cleavage mediated by furin (Louvi and Artavanis-Tsakonas, 2012). In the absence of the ligand, a negative regulatory region (NRR), comprising the Lin12-Notch repeats and the heterodimerization domain, keep the receptor in an autoinhibited configuration stabilized via noncovalent bonds (Xu et al., 2015). Interactions with Notch ligands (Delta or Jagged) expose an S2 cleavage site within the NRR to proteolysis by ADAM (a disintegrin and metalloproteinase domain; Louvi and Artavanis-Tsakonas, 2012; Xu et al., 2015). Presenilin-containing γ-secretase constitutively cuts S2-cleaved

*A.I. Machuca-Parra and A.A. Bigger-Allen contributed equally to this paper.

Correspondence to Joseph F. Arboleda-Velasquez: joseph_arboleda@meei.harvard.edu; Patricia A. D'Amore: patricia_damore@meei.harvard.edu

Abbreviations used: Bt, biotinylated; CADASIL, cerebral autosomal-dominant arteriopathy with subcortical infarcts and leukoencephalopathy; Cre, causes recombination; Flp, flippase; FRT, flippase recognition target; HEK, human embryonic kidney; MC, mural cell; N3ECD, Notch3 extracellular domain; NRR, negative regulatory region; P, postnatal day; SA-HRP, streptavidin-HRP conjugate; SMA, α-smooth muscle actin; SVD, small vessel disease; TEM, transmission electron microscopy; TET, tetracycline; TNB, Tris-NaCl-blocking buffer.

The Rockefeller University Press
J. Exp. Med. 2017 Vol. 214 No. 8 2271–2282
https://doi.org/10.1084/jem.20161715

Notch receptors at a transmembrane site (S3), leading to nuclear translocation of the Notch intracellular domain and regulation of transcriptional downstream targets (Kopan, 2012).

Here, we tested a modality of treatment focused on preventing mural cell loss, a mechanistic cause of CADASIL (Chabriat et al., 2009) and a hallmark of other SVDs, including diabetic retinopathy (Arboleda-Velasquez et al., 2015). For that purpose, we used mouse models with *Notch3* mutations (Arboleda-Velasquez et al., 2008, 2011) and a Notch3 agonist antibody (Li et al., 2008). To examine the efficacy of the treatment, we leveraged a roster of morphological and blood biomarkers previously characterized in a CADASIL mouse model, including mural cell coverage in arteries and changes in plasma levels of Notch3 extracellular domain (N3ECD), high-temperature requirement A serine peptidase 1 (HTRA1), collagen 18α1/endostatin, and insulin-like growth factor binding protein 1 (IGFBP-1; Primo et al., 2016).

RESULTS AND DISCUSSION

Mural cell coverage in vessels is mechanistically linked to Notch3 signaling

To investigate cell autonomous effects of Notch3 signaling in mural cells, we examined mural cell coverage in retinal vessels from Notch3 knockout (N3KO) mice and N3KO mice in which conditional expression of WT or mutant human *NOTCH3* transgenes was driven from the ROSA26 (reverse orientation splice acceptor 26) locus (Soriano, 1999) using Cre (causes recombination) recombinase under the smooth muscle cell promoter SM22 (smooth muscle protein 22; Fig. 1 A; Holtwick et al., 2002). The retina has a very stereotypic vessel distribution with a blood barrier similar to that of the brain and, therefore, offers unique advantages for quantitative assessments of changes in vascular structure associated with *Notch3* mutations (Henshall et al., 2015; Kofler et al., 2015). Moreover, there is clinical evidence for retinal changes in patients with CADASIL affecting the superficial retinal vessels feeding the retinal nerve fiber layer (Robinson et al., 2001; Roine et al., 2006; Rufa et al., 2011). Morphometric software separated main and branching vessel analyses, quantifying α-smooth muscle actin (SMA) coverage in both (Fig. S1). We chose SMA staining to detect mural cells because expression of this marker is not affected by changes in Notch3 activity, whereas the expression of other markers of mural cells, including neuron-glial antigen 2, platelet-derived growth factor receptor β, and desmin, are regulated by Notch3 signaling (Arboleda-Velasquez et al., 2008, 2014; Jin et al., 2008).

We found that absence of Notch3 expression dramatically reduced mural cell coverage in superficial retinal arteries and arterioles of 6-mo-old animals (Fig. 1, B and C). Despite this robust loss of mural cells, Notch3 knockout animals did not show detectable abnormalities in retinal function assessed via electroretinogram (not depicted). Expression of WT human NOTCH3 transgene (hN3WT) was sufficient to rescue mural cell loss in both large vessels and smaller caliber arteriole branches of N3KO mice (Fig. 1, B and C). Confirming our immunohistologic findings, transmission electron microscopy (TEM) showed large gaps in mural cell coverage in vessels from the brain cortex and the retina in N3KO mice, whereas mural cells were juxtaposed to each other in knockout animals expressing human Notch3 in mural cells (Fig. 1, D and E). We detected mural cells undergoing apoptosis within the arterial gaps in N3KO animals in the retina and the brain (Fig. 1, F and G).

We further investigated the effect of human Notch3 receptor with the C455R mutation on mural cells because that mutation was identified in a CADASIL family with early age at onset of stroke and extensive magnetic resonance imaging abnormalities and can impair ligand-mediated Notch3 signaling (Arboleda-Velasquez et al., 2002, 2011). Expression of the C455R allele in mice led to the formation of granular osmiophilic material (Arboleda-Velasquez et al., 2011); however, like other previously reported CADASIL models (Joutel et al., 2010; Joutel, 2011; Wallays et al., 2011), these mice did not develop morphological signs of spontaneous stroke or brain parenchymal changes by 6 mo of age (not depicted; Arboleda-Velasquez et al., 2011). Immunohistology and TEM analysis showed that unlike the hN3WT, expression of CADASIL mutant (C455R) human *Notch3* transgene did not rescue the mural cell loss in N3KO animals, a finding consistent with this mutation causing a loss of function (Arboleda-Velasquez et al., 2011). Surprisingly, the mural cell loss phenotype did not appear to be worse in N3KO animals expressing the C455R mutant than in N3KO animals not expressing the CADASIL mutant *Notch3* (Fig. 1 C). This suggests that neomorphic effects, previously reported for CADASIL mutations (Joutel et al., 2016), likely do not contribute to mural cell loss in mice carrying the C455R mutation at the 6-mo point. Whether CADASIL mutant *Notch3* receptors contributes to mural cell loss with aging or whether there is a phenotype in SMA-negative pericyte populations deserves further investigation. Examining the latter will require the identification of pericyte markers that are not affected by Notch3 signaling to obtain unambiguous results.

Mural cell loss impairs blood-barrier integrity in the central nervous system resulting in increased vascular permeability (Armulik et al., 2010; Valdez et al., 2014). We conducted retinal fluorescence angiography in live mice to assess the functional consequences of mural cell loss in our mouse models. N3KO and C455R mice showed a significant increase in vascular leakage consistent with their robust mural cell loss, whereas those events were less frequent in N3KO expressing the hN3WT allele, indicating functional rescue (Fig. 2). Expression of the hN3WT transgene was also able to rescue the leakage phenotype in N3KO expressing the C455R mutant transgene, a cohort of mice resembling a heterozygote condition (Fig. 2).

Altogether, these findings indicate that Notch3 signaling is both necessary and sufficient to support mural cell coverage in arteries via cell-autonomous effects.

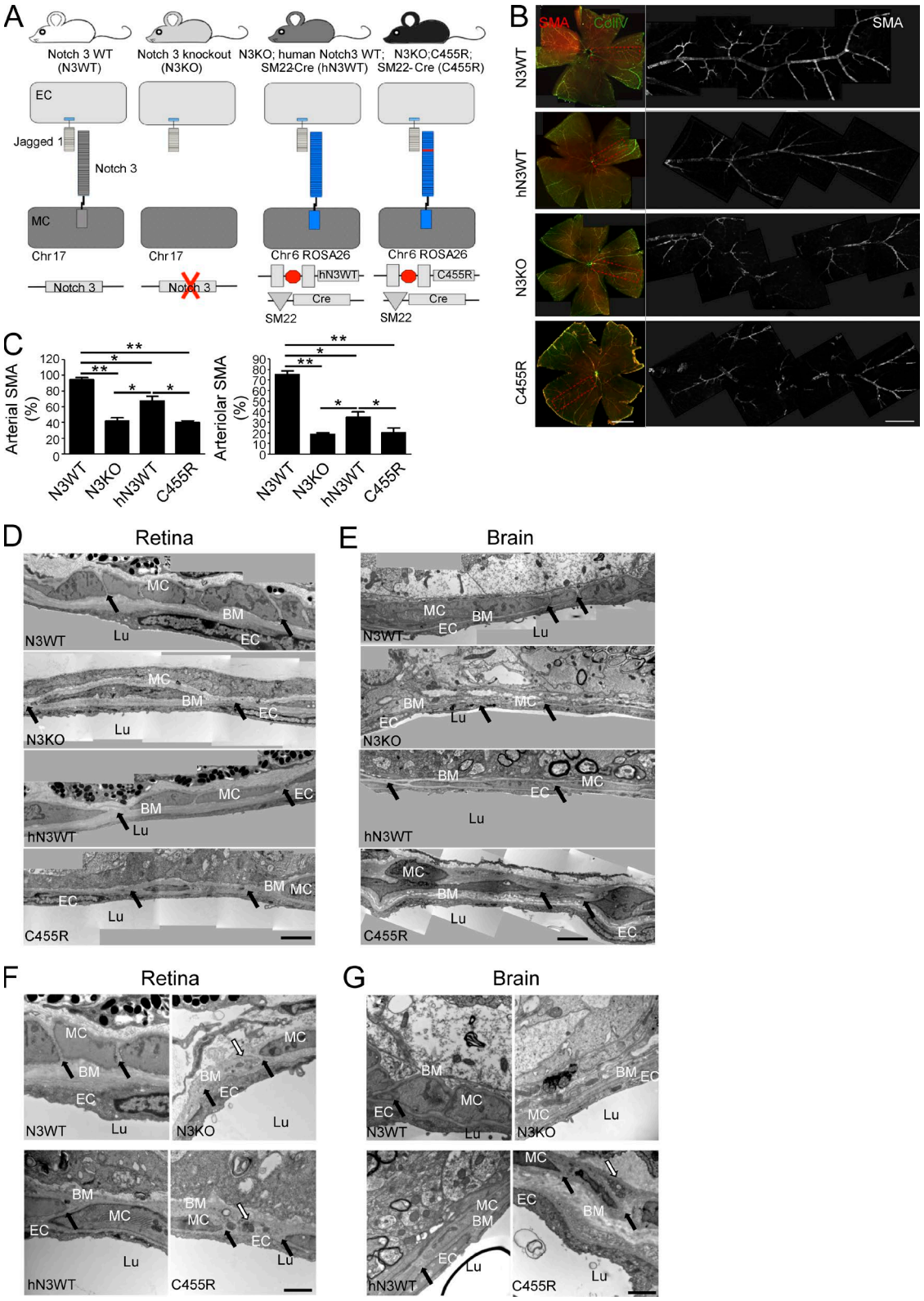

Figure 1. **Human Notch3 rescues mural cell loss in N3KO mice.** (A) Schematic representation of four mouse strains used to study genetic rescue of Notch3 signaling: WT Notch3 (N3WT, white), Notch3 knockout (N3KO, light gray), mice conditionally expressing WT human Notch3 (hN3WT, dark gray), and mice conditionally expressing a human CADASIL mutant Notch3 (C455R, black). (B) Representative immunofluorescence images of retinal whole mounts showing SMA staining in red and white and ColIV in green (left; bar, 2.5 mm). Red, dashed rectangles (left) indicate regions displayed in right (bar, 250

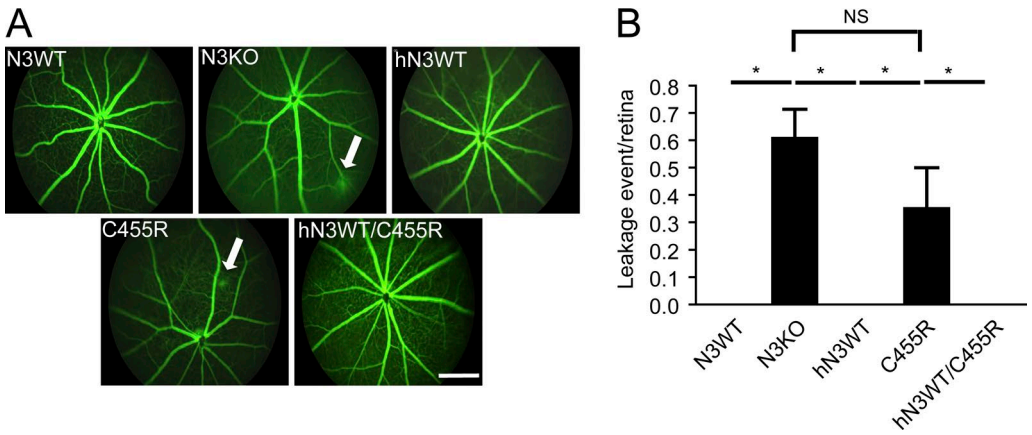

Figure 2. **Human Notch3 rescues vascular leakage in N3KO and CADASIL mice.** (A) Fluorescein angiography images of mouse retinas from the listed genotypes: N3WT, N3KO, hN3WT, C455R, and mice conditionally expressing hN3WT and C455R as heterozygotes (C455R/hN3WT). Arrows mark leakage events (bar, 300 µm). (B) Graph shows quantification of leakage events in N3WT (n = 6), N3KO (n = 6), hN3WT (n = 5), C455R (n = 3), and C455R/hN3WT (n = 5) mice. Values in graph are expressed as the means ± SEM *, $P < 0.05$. Data were analyzed via ANOVA. N3KO, C455R, hN3WT, and C455R/hN3WT were littermates. N3WT mice were bred separately in house. (A and B) The results are representative of two independent experiments.

A Notch3 agonist antibody activates a ligand-insensitive, mutant Notch3 receptor in vitro

Genetic rescue in N3KO mice and in N3KO expressing the C455R mutant Notch3 by hN3WT supports the notion that patients with SVD because of misregulated Notch3 signaling may benefit from therapeutic approaches leading to Notch3 signaling normalization. We sought to further test this hypothesis by evaluating the therapeutic potential of an agonist antibody (A13) specific for the Notch3 receptor's NRR located in the receptor's extracellular domain (Fig. 3 A; Li et al., 2008; Xu et al., 2015). We chose to focus on the C455R mutation because it results in very strong abrogation of Notch3 signaling compared with other CADASIL mutations (Fig. 3; Arboleda-Velasquez et al., 2011).

For in vitro testing of the A13 agonist antibody, we generated isogenic human embryonic kidney (HEK) 293 cell lines expressing the human Notch3 receptor (WT or C455R mutant) and cells expressing the human Jagged 1 Notch ligand under the control of a tetracycline (TET)-inducible promoter. This design ensured comparable levels of transgene expression between mutant and WT Notch3 and prevented potential confounding effects of uncontrolled overexpression. Jagged 1 is a functional ligand for Notch3 in vivo (High et al., 2008). We transfected Notch3-expressing cells with TP1 (Epstein Barr virus terminal protein 1)-Luciferase (Zimber-Strobl et al., 1994), a reporter of Notch transcriptional activity, before co-culture with Jagged 1–expressing cells in the presence of TET. Using this Notch signaling reporter assay, we found that the A13 antibody induced activation of the WT and the C455R mutant Notch3 receptors in monocultures (Fig. 3, B and C) and in co-cultures of receptor-expressing cells, with cells expressing the Jagged 1 ligand (Fig. 3, D–I). As expected, Jagged 1–expressing cells activated signaling in WT Notch3–expressing cells, whereas they failed to activate signaling in cells expressing the C455R mutant receptor (Fig. 3, D and E). These results indicate that the Notch3 agonist antibody is capable of activating a Notch3 receptor rendered insensitive to the Jagged 1 Notch ligand activation by the C455R CADASIL mutation, a finding with translational potential. In addition, effective activation in the presence and the absence of Jagged 1 suggests a noncompetitive mechanism.

N3ECD is present in mouse and human plasma and its levels are reduced in mice carrying the C455R *Notch3* mutation (Primo et al., 2016). We tested whether N3ECD was detectable in cell culture supernatants and whether its levels changed upon activation. Incubation of WT and C455R cells with the Notch3 agonist led to a significant increase of N3ECD in the cell culture supernatant, consistent with the

µm). (C) Quantification of SMA coverage in main retinal arteries and branching arterioles. n = 5 for each group. *, $P < 0.05$; **, $P < 0.01$; statistical analysis was performed via ANOVA. Values in graphs are expressed as means ± SEM. The results are representative of two independent experiments. Ultrastructural images of retinal vessels (D; bar, 20 µm) and cerebral vessels (E) from the left hemisphere of the cerebral cortex, cut at the bregma (bar, 20 µm) obtained by TEM. Lumen (Lu), vascular endothelial cell (EC), basement membrane (BM), mural cell (MC), gaps in MC (black arrows), and apoptotic bodies (white arrows) are shown. Similarly, the same six features are highlighted on each image from retina (F) and brain (G; bars, 1 µm). The N3WT mice exhibit large, block-like MC that are in contact or are closely associated, whereas the N3KO and C455R mice exhibit large gaps and elongated MCs. hN3WT exhibits elongated MCs juxtaposed to each other. (D–G) Images are representative of three mice analyzed for each genotype. N3KO, C455R, and hN3WT were littermates. N3WT mice were bred separately in house. (B, D, and E) Images tracing vessels were stitched together to generate the complete picture.

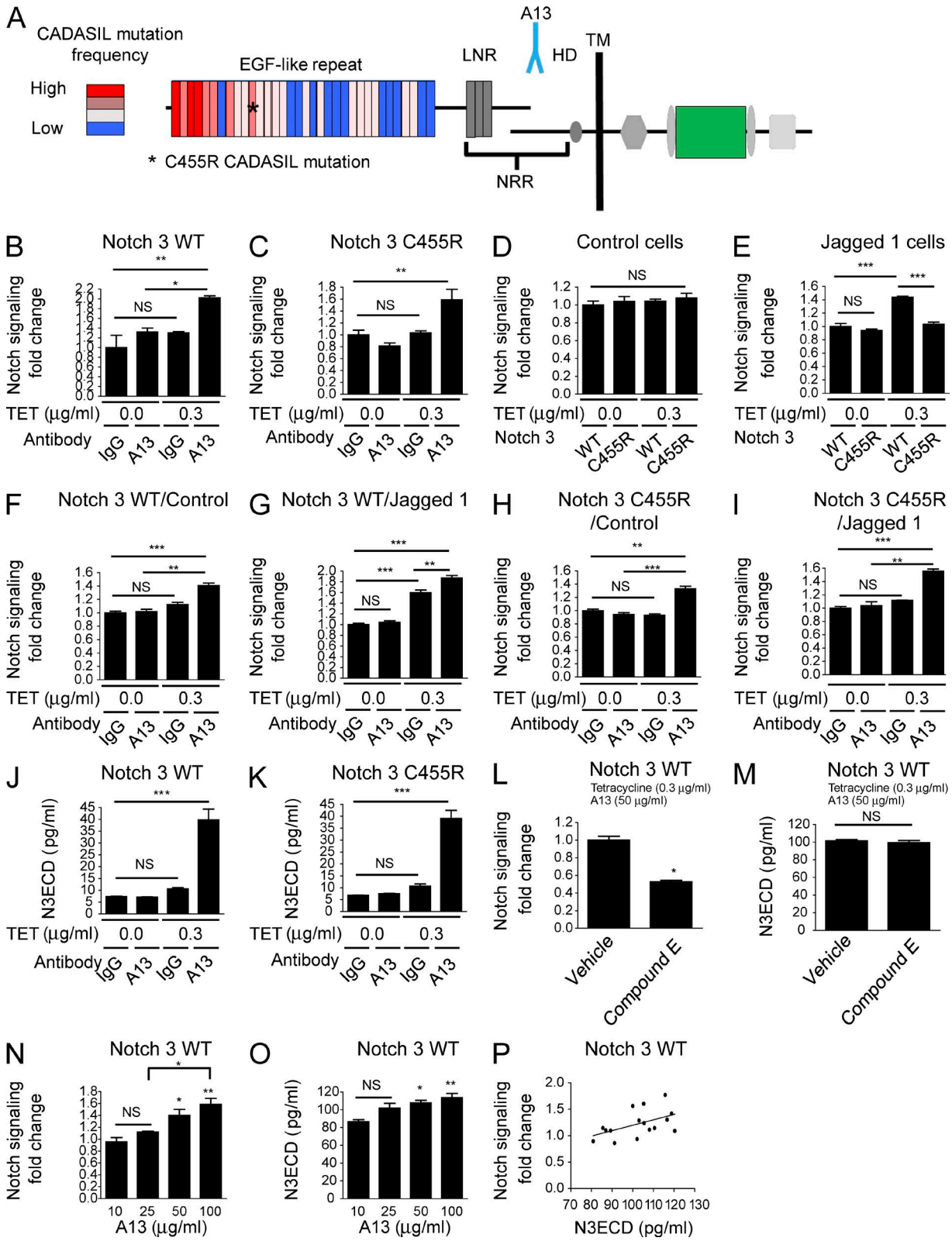

Figure 3. **A13 Notch3 agonist antibody activates a ligand-insensitive Notch3 receptor with the C455R mutation in vitro.** (A) Schematic diagram showing the structure of the Notch3 receptor and the binding site where the A13 antibody interacts with the NRR domain. Lin12-Notch (LNR), heterodimerization domain (HD), and transmembrane domain (TM) are shown. Luciferase reporter assay for Notch signaling in monocultures of HEK 293

notion that A13 activates Notch3 by destabilizing the receptor's NRR in a ligand-independent manner, leading to exposure of the S2 cleavage site (Fig. 3, J and K; Li et al., 2008). As expected, treatment with compound E, a γ-secretase inhibitor, was able to reduce Notch3 signaling mediated by the A13 antibody but had no significant effects on the levels of N3ECD released into the supernatant (Fig. 3, L and M). Interestingly, Notch3 signaling activation measured via a gene reporter assay correlated with increased levels of N3ECD in cell culture supernatants measured by ELISA (R^2 = 0.8231, P = 0.049; Fig. 3, N–P). This finding is relevant because it indicates that the levels of N3ECD in liquid biopsies could be used as a surrogate marker of Notch3 activity for diagnostic and prognostic purposes and in clinical trials. Currently, there are no straightforward alternatives to measure Notch signaling in vivo.

Notch3 activation prevents mural cell loss in a mouse model of CADASIL

We then tested the A13 Notch3 agonist antibody in vivo using morphological and molecular signatures previously reported in C455R mice (Primo et al., 2016) as primary end points to assess the efficacy of treatment. 6-mo-old C455R mice had reduced mural cell coverage in retinal arteries and arterioles (Fig. 1, B and C), reduced plasma levels of N3ECD, and increased plasma levels of HTRA1, IGFBP-1, and endostatin/collagen 18α1, compared with control mice (Primo et al., 2016). Rescue of mural cell coverage in small or large vessels was included as required, prespecified criteria for efficacy because mural cell loss is a hallmark of SVD and because we showed this variable depended on Notch3 signaling in our models (Fig. 1, B and C). We also deemed it essential to include reversal of at least one blood biomarker as required, prespecified criteria for efficacy because blood biomarkers could potentially be measured in a clinical trial.

Mice were injected i.p. with A13 or an isotype control (IgG), for 5 wk starting at postnatal day 8 (P8; Fig. 4 A). Antibodies penetrated the blood–retinal barrier after perfusion at discrete perivascular sites (Fig. S2), indicating bioavailability at the appropriate compartment. We found that administration of A13 resulted in about double the extent of SMA coverage in retinal arterioles in 6-wk-old mice (Fig. 4, B and C). No effect was detected on SMA coverage in large retinal arteries (Fig. 4, B and C). As expected, no effect was observed in Notch3 knockout mice treated with control and agonist antibody (Fig. 4, B and C). Vascular density was not significantly different across conditions, and our analysis of specificity and efficiency of SM22-Cre–mediated recombination demonstrated expression of the human Notch3 protein in small and large vessels in C455R animals (Fig. S3). Whether the lack of a detectable effect in large retinal arteries reflects differential sensitivity to Notch3 signaling in mural cells from large versus small vessels deserves further investigation.

To examine target engagement by the A13 agonist across the blood-brain barrier, we stained brain tissues with a novel antibody shown to be specific for active (S3-cleaved) Notch3 (V1662; Choy et al., 2017). Brain vessels from C455R mice injected with A13 stained with V1662, whereas no staining was detected in C455R mice injected with control IgG (Fig. 4 D).

N3ECD and endostatin/collagen 18α1 are surrogate markers of Notch3 activity in vivo

Plasma levels of N3ECD and endostatin/collagen 18α1 increased in mice injected with the A13 agonist antibody, whereas IGFBP-1 and HTRA1 did not change significantly compared with the control (Fig. 5). Increased N3ECD in the plasma of mice injected with A13 is consistent with our in vitro work linking this biomarker to increased Notch3 signaling (Fig. 3). Endostatin/collagen 18α1 expression is regulated by Notch3 transcriptional activity (Primo et al., 2016). Age of the animal also affects the levels of this biomarker in plasma (Primo et al., 2016). In 100-d-old mice, C455R plasma endostatin/collagen 18α1 was reduced, whereas it was increased in 6-mo-old C455R mice (Primo et al., 2016). Based on this precedent, we concluded that the increase in endostatin/collagen 18α1 in 6-wk-old C455R mice treated with A13 agonist was linked to increased Notch3 signaling. Altogether, these analyses indicate that N3ECD and endostatin/collagen 18α1 in plasma are sensitive surrogate markers of Notch3 activity in vivo.

We conclude that restoring Notch3 signaling in mural cells via genetic manipulations or using a Notch3 agonist is effective at preventing SVD phenotypes in Notch3 knockout

cells expressing Notch3 WT receptor (B) or the Notch3 C455R (C) after treatment with A13 or control IgG antibodies. TET indicates concentration of tetracycline used to induce transgene expression. Luciferase reporter assay for Notch signaling in HEK 293 cell co-cultures. HEK 293 cells expressing Notch3 WT or C455R Notch3 receptors in co-culture with control cells (D) or with HEK 293 cells expressing Jagged 1 (E). HEK 293 cells expressing Notch3 WT in co-culture with control cells (F) or with cells expressing Jagged 1 (G) treated with IgG or A13 antibodies. HEK 293 cells expressing Notch3 C455R in co-culture with control cells (H) or with cells expressing Jagged 1 (I) treated with IgG or A13. ELISA measurements of N3ECD in cell culture supernatant for each culture, Notch3 WT (J) and C455R (K). Luciferase reporter assay for Notch signaling in monocultures of HEK 293 cells expressing Notch3 WT receptor in the presence of compound E (L). ELISA measurements of N3ECD in cell culture supernatant in the presence of compound E (M). Luciferase reporter assay for Notch signaling in monocultures of HEK cells expressing Notch3 WT receptor treated with increasing concentrations of A13 (N). ELISA measurements of N3ECD in cell culture supernatant from cells treated with increasing concentrations of A13 (O). Notch3 signaling activation measured via gene reporter assay correlated with increased levels of N3ECD in cell culture supernatants measured by ELISA (P). (B–P) *, P < 0.05; **, P < 0.01; ***, P < 0.001. Data were analyzed via ANOVA. Values in graphs are expressed as the means ± SEM. The results are representative of three independent experiments each including three technical replicates per condition.

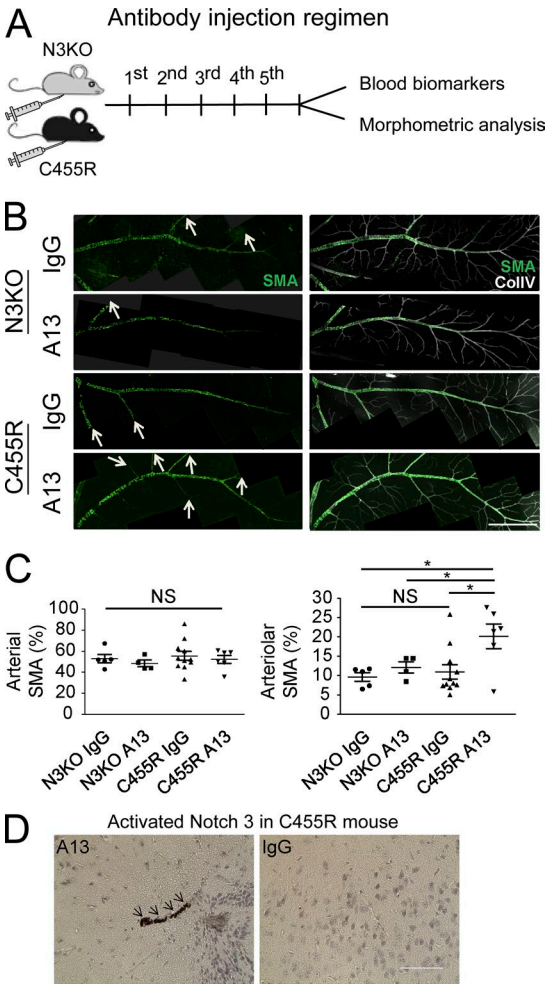

Figure 4. **A13 Notch3 agonist antibody prevents mural cell loss in CADASIL mice.** (A) Timeline of A13 antibody injections in N3KO (light gray) and CADASIL mutant mice (black). (B, left) Representative immunofluorescence images of retinal whole mounts showing SMA staining in green for N3KO and C455R mutant mice treated with IgG or A13 antibodies. (Right) Merged images of green and white signals (ColIV staining; bar, 100 µm). Arrows show small-caliber vessels with SMA coverage for each genotype. Images tracing vessels were stitched together to generate the complete picture. (C) Quantification of SMA coverage in retinal vasculatures from N3KO (IgG treated, $n = 5$; A13 treated, $n = 4$) and C455R (IgG treated, $n = 11$; A13 treated, $n = 6$) from 10 independent rounds of injections. Each data point represents the value for a single mouse. Horizontal lines show the means ± SEM *, $P < 0.05$. Data were analyzed via ANOVA. The C455R and N3KO mice were littermates. (D) Images of brain tissue from C455R injected with A13 or IgG antibody stained with V1662 antibody. C455R IgG ($n = 3$) and C455R A13 ($n = 3$). Bar, 100 µm. The results are representative of two independent experiments.

and CADASIL mice. Furthermore, we identified N3ECD and endostatin/collagen 18α1 as blood biomarkers indicative of effective modulation of Notch3 activity in vivo. Although further preclinical and clinical testing are necessity, our findings may be of significance for patients with hypomorphic CADASIL mutations in *Notch3* and also for individuals with other SVD conditions mechanistically linked to Notch3 loss of function.

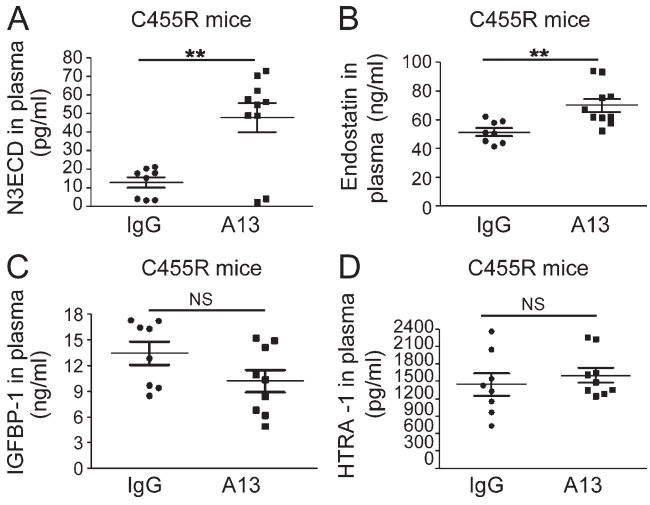

Figure 5. **A13 Notch3 agonist antibody reverses plasma biomarker changes in N3ECD and endostatin/collagen 18α1 in CADASIL mice.** Dot plots showing plasma levels of N3ECD (A), endostatin/collagen 18α1 (B), IGFBP-1 (C), and HTRA1 (D) in 6-wk-old C455R mice treated with the A13 ($n = 10$) or IgG ($n = 8$) antibodies from 10 independent rounds of injections. (A-D) **, $P < 0.01$. Statistical analysis was done via unpaired two-tailed Student's *t* test. Each data point represents the value for a single mouse. Horizontal lines show the means ± SEM. The C455R mice were littermates.

MATERIALS AND METHODS

Study approval

The Schepens Eye Research Institute Institutional Animal Care and Use Committee approved this study. All procedures followed were in accordance with institutional guidelines.

Statistical analyses. Pairwise comparisons were assessed using an unpaired two-tailed Student's *t* test. One-way ANOVA was used to compare more than two experimental groups. Results were considered significant for $P < 0.05$. Linear regression analysis was performed to measure correlation Notch3 signaling and the levels of N3ECD in cell culture supernatant. Analyses were performed and displayed using Prism software (GraphPad Software).

Generation of cell lines. HEK 293 cells stably expressing the Notch3 WT receptor, Notch3 C455R receptor, and Jagged 1 WT ligand under a TET-inducible promoter were generated using the Flp-In T-REx HEK system (Thermo Fisher Scientific) according to the supplier's protocol. In brief, expression vectors containing each of those transgenes (pCDNA5/FRT/TO-hNotch3WT, pCDNA5/FRT/TO-hNotch3C455R, and pCDNA5/FRT/TO-hJagged1WT) were integrated into the genome via flippase (Flp) recombinase-mediated DNA recombination at an FRT (flippase recognition target) site in HEK 293 cells. These cells were authenticated by having resistance to the

expected antibiotics and by carrying the expected transgenes allowing for Flp recombination. For this purpose, 5.5 million Flp-In T-REx HEK cells were plated into a 100-mm dish for each construct and incubated overnight using "complete medium" (DMEM [Lonza], supplemented with 10% FBS [Atlanta Biologicals], 2 mM L-glutamine [Lonza], 100 U/ml penicillin, 100 µg/ml streptomycin [Lonza], 100 µg/ml Zeocin [Thermo Fisher Scientific], and 15 µg/ml blasticidin [Thermo Fisher Scientific]). The next day, the medium was aspirated, and 10 ml of "transfection medium" (DMEM [Gibco and Lonza], supplemented with 10% FBS [Atlanta Biologicals]) was added. Cells were cotransfected with 14 µg of the pOG44 vector and 2 µg of the desired constructs in 1 ml of OptiMEM (reduced-serum medium; Lonza) and 40 µl of lipofectamine 2000 (Invitrogen) in 1 ml of OptiMEM per plate for transfection, using the provider's protocol. A negative control (no DNA) was included during the experiment. After 48 h, the medium was aspirated and replaced with "selection medium" (DMEM [Lonza], supplemented with 10% FBS [Atlanta Biologicals], 2 mM L-glutamine [Lonza], 100 U/ml penicillin, 100 µg/ml streptomycin [Lonza], 150 µg/ml hygromycin [Invitrogen], and 15 µg/ml blasticidin [Invitrogen]). The medium was changed every third day until the control cells died and colonies formed for transfected cells. Colonies were detached with trypsin Versene (Lonza) and plated in selection media.

Cell cultures, transfections, and gene reporter assays. Flp-In T-REx HEK cells were cultured using complete medium (previously described), and HEK cells expressing the Notch3 WT, Notch3 C455R receptors, and the Jagged 1 WT ligand were grown in selection medium (previously described). All cultures were maintained at 37°C and 5% CO_2. All vectors were purified with the Plasmid Midi kit (QIAGEN). At least two independent plasmid preparations were used for transfection. For transfections, 4×10^5 cells per well (HEK cells expressing the Notch3 WT and Notch3 C455R receptors) were plated into 12-well plates with selection medium. The next day, the selection medium was replaced by transfection medium (previously described) and OptiMEM (Lonza), using 1.5 µg of the Epstein-Barr virus terminal protein 1–luciferase plasmid (Zimber-Strobl et al., 1994), and 0.125 µg CMV promoter-driven *Renilla* luciferase construct (pRL-CMV; Promega) to normalize the transfection efficiency. Transfections were performed using 4 µl per well of lipofectamine 2000 (Thermo Fisher Scientific) in OptiMEM. After 8 h, the transfection medium was replaced with "experimental medium" (DMEM [Lonza], supplemented with 1% TET-free FBS [Takara Bio Inc.], 2 mM L-glutamine [Lonza], 100 U/ml penicillin, and 100 µg/ml streptomycin [Lonza]). 4×10^5 cells in experimental medium (HEK cells expressing Jagged 1 WT and TRex HEK cells as a control) were added per well. To induce expression of the receptors (Notch3 WT and Notch3 C455R) and the ligand (Jagged 1 WT), 0.3 µg/ml of TET were added. A no-TET condition was included as a control. For the antibody assays, cells were exposed to 50 µg/ml of the A13 or IgG for 48 h then harvested to measure luciferase activity with a luminometer (TD-20/20; Turner Designs) with the Dual-Luciferase reporter assay system (Promega). We conducted experiments in the presence of 100 nM of compound E (Enzo Life Sciences) or DMSO (vehicle), including 0.3 µg/ml of TET and 50 µg/ml of the A13. For the antibody dose curve, four different concentrations of the A13 antibody (10, 25, 50, and 100 µg/ml) were used in the presence of 0.3 µg/ml of TET. Three independent experiments were conducted for each dataset.

Animal models. All mouse models used in this study were previously described and were backcrossed to C57BL/6 background for seven generations (Mitchell et al., 2001; Arboleda-Velasquez et al., 2008, 2011). Both male and female littermates were included in the study. In brief, mice were either WT (N3WT), lacking endogenous mouse Notch3 (N3KO), or expressed either a WT human *NOTCH3* transgene (hN3WT, MMRRC:032998 B6;129 *Gt(ROSA)26Sor*$^{tm1(NOTCH3)Sat}$/Mmjax) or a mutated human *NOTCH3* transgene (C455R, MMRRC:033000 129-*Gt(ROSA)26Sor*$^{tm2(NOTCH3*C455R)Sat}$/Mmjax) in an N3KO background. The hN3WT and C455R mouse models are available from The Jackson Laboratory under the auspices of the Mutant Mouse Regional Resource Centers program and U.S. National Institutes of Health.

Study design for in vivo experiments

Five mice per experimental group were expected to detect a difference of 30% between the means with 80% power (α = 0.05) based on a previously published SD of 14% for mural cell coverage (Primo et al., 2016). The identity of the antibody was unknown to the investigators during the injections and data analysis. Specific litters were assigned to either treatment randomly in independent experiments. Prespecified primary endpoints for analyses included two morphological measures (SMA coverage in arteries and arterioles) and four published blood biomarkers (N3ECD, HTRA1, IGFBP-1, and endostatin/collagen 18α1; Primo et al., 2016). Efficacy was prespecified as a significant increase in SMA coverage in either arteries or arterioles *and* reversal of at least one blood biomarker. No post hoc analyses were conducted after the mask was lifted. Variations in sample size between groups occurred because injections began at P8, before the earliest time that Institute Institutional Animal Care and Use Committee regulations allowed us to collect mouse biopsies for genotyping (P15). No outlier data points were removed for analysis. Differences in sample size between morphometric and blood protein variables arose because of low-quality dissection or staining of eyes. These eyes were removed from the analysis before lifting the mask.

Mouse cohorts and antibody injections. Two cohorts of N3WT, N3KO, hN3WT, and C455R mice were used for this study. The first cohort was euthanized at 6 mo before tissue analysis. The second cohort included P8 N3KO and C455R

mice injected i.p. with either an anti–human Notch3 agonist (A13), generated using hybridoma technology from Genentech, or an anti–ragweed control antibody, also from Genentech, once a week for 5 wk. Mice were grouped from 10 independent rounds of injections with A13 or IgG after the mask was lifted. Requests for access to these antibodies (and for V1662 antibody listed below) should be directed to the Genentech material-transfer agreement program (mta-d@gene.com). A dose of 30 mg/kg antibody to the mass of animal was injected in sterile PBS. At P8 and P15, the concentration of the antibody was higher (1.0 mg/ml) than it was when injected afterward (0.333 mg/ml) to reduce the amount of PBS injected. The mice were then sacrificed on the sixth week; at which point, blood and tissue were collected. The A13 antibody was labeled with ReadiLink 647/674 antibody labeling kit (1351006; Bio-Rad Laboratories) to study antibody penetration across the blood–retinal barrier. Antibody penetration was examined in the retina 6 h after i.p. injection of labeled antibody and transcardial perfusion with 4% PFA in PBS.

Immunofluorescence. Eyes were harvested from 6-wk-old, injected animals or 24-wk-old animals and fixed in 4% PFA overnight at 4°C. The eyes were then washed three times in PBS (D5652-10 × 1L; Sigma-Aldrich); at which point, retinas were dissected from each eye and washed as described above. Retinas were then placed in borosilicate glass vials (16218–126; VWR International) and 300 µl of blocking buffer for 6 h. Blocking buffer was prepared, as previously described (Primo et al., 2016). Retinas were washed again as above and were double stained with primary antibodies against goat anti–mouse SMA (NB300-978; Novus Biologicals) at 1:100 concentration, rabbit anti–mouse collagen IV (ab6586; Abcam), and mouse anti–human Notch3 (clone 1E4, MABC594; EMD Millipore) in blocking buffer overnight at 4°C on a rocker. Retinas were then washed as described above and immersed for 4 h at room temperature in secondary antibodies: donkey anti–goat IgG H&L (Cy3) preadsorbed (ab6949; Abcam), donkey anti–rabbit IgG H&L (Alexa Fluor 488, ab150073; Abcam), donkey anti–mouse IgG H&L (Alexa Fluor 647, ab150107; Abcam), all at a 1:100 concentration in blocking buffer. Retinas were then washed as described above and whole mounted on glass slides, (EMSC200L; Azer Scientific), coated with 50% glycerol in PBS under a rectangular coverslip (12–545-F; Thermo Fisher Scientific), and sealed with nail polish (8435–76; Revlon, Inc.). Entire retinas were imaged at 5 × 1.25 magnification, and three vessels from each retina were imaged at 20 × 1.25 magnification with an Axioscope 2 Mot Plus (ZEISS).

Electron microscopy. After transcardial perfusion, mouse eyes and brain tissue were immersed, fixed with half strength Karnovsky's fixative (2% formaldehyde + 2.5% glutaraldehyde, in 0.1 M sodium cacodylate buffer, pH 7.4; Electron Microscopy Sciences) at room temperature. An eyecup was created from each eye by dissecting away the anterior from the posterior ends. Posterior eyecup and brain samples were then placed back into half-strength Karnovsky's fixative for a minimum of 24 h under refrigeration. After fixation, samples were rinsed with 0.1 M sodium cacodylate buffer, postfixed with 2% osmium tetroxide in 0.1 M sodium cacodylate buffer for 1.5 h, en bloc stained with 2% aqueous uranyl acetate for 30 min, then dehydrated with graded ethyl alcohol solutions, transitioned with propylene oxide and resin infiltrated in tEPON-812 epoxy resin (tousimis) using an automated Lynx 2 EM tissue processor (Electron Microscopy Sciences). The processed samples were oriented into tEPON-812 epoxy resin inside flat molds and polymerized in a 60°C oven. Semithin sections were cut at 1 µm thickness through the midequatorial plane, traversing the optic nerve in the posterior eyecup samples, and stained with 1% toluidine blue in 1% sodium tetraborate aqueous solution for assessment by light microscopy. Ultrathin sections (80 nm) were cut from each sample block using an EM UC7 ultramicrotome (Leica Biosystems) and a diamond knife, then collected using a loop tool onto either 2 × 1-mm, single-slot formvar-carbon–coated or 200-mesh–uncoated copper grids, and air-dried. The ultrathin sections on grids were stained with aqueous 25% uranyl acetate replacement stain (Electron Microscopy Sciences) and Sato's lead citrate using a modified Hiraoka grid-staining system. Grids were imaged using a Tecnai G2 Spirit transmission electron microscope (FEI Company) at 80 kV, interfaced with an AMT XR41 digital CCD camera (Advanced Microscopy Techniques) for digital TIFF (tag image file format) file image acquisition. TEM imaging of vessels in both retina and brain samples were assessed, and digital images were captured at 2,000 × 2,000 pixels, 16-bit resolution.

Fundus photography and fluorescein angiography. A Micron III (Phoenix Research Labs) system was used to take fundus photographs in anesthetized mice, according to the manufacturer's instructions. The animals' pupils were dilated using a drop of 1% tropicamide, followed by a drop of 1% cyclopentolate hydrochloride applied on the corneal surface. Eyes were kept moist with ocular lubricant (Geneal; Novartis). Fluorescein angiography was performed after i.p. injection of 0.05 ml of 25% fluorescein sodium (pharmaceutical grade; Akron). Photographs were taken with a preset 20D lens appositioned to the camera lens at regular time (from 1 to 4 min after i.p. injection).

Immunohistochemistry. Brains were fixed in 10% formalin in Dulbecco's PBS (1×; 137 mM NaCl, 2.7 mM KCl, 8 mM Na_2PO_4, 1.47 mM KH_2PO_4, pH 7.4) overnight at room temperature and stored in PBS at 4°C until paraffin embedding. Serial sections (6 µm) were cut, deparaffinized in 100% xylene, and hydrated and rinsed with distilled water. Sections were place in 65°C target antigen retrieval solution, and then, the temperature was raised to 99°C, and the sections were incubated for 20 min, followed by a 20-min cool-down pe-

riod (74°C). Sections were rinsed with distilled water and then blocked for 4 min at room temperature using the KPL blocking solution (1:10 in distilled water) to quench endogenous peroxidase activity. Sections were rinsed with TBS and Tween 20 (TBST) and then blocked with a vector/biotin blocking kit, following the manufacturer's instructions. Sections were rinsed with TBST and then blocked with Tris-NaCl blocking buffer (TNB) buffer for 30 min at room temperature. Sections were incubated with the primary anti-Notch3 intracellular domain antibody (5 µg/ml in blocking serum GNE, V1662; Genentech) for 60 min at room temperature. IgG was used as a negative control (5 µg/ml in blocking serum). Sections were rinsed with TBST and then incubated in biotinylated (Bt)-donkey anti–rabbit at 5 µg/ml for 30 min at room temperature, then rinsed with TBST and followed by an incubation in the streptavidin-HRP conjugate (SA-HRP) for 30 min at room temperature (1:100 in TNB buffer; PerkinElmer). Sections were rinsed twice with TBST and then incubated in Bt-tyramide for 3 min at room temperature (1:50 in amplification buffer; PerkinElmer). Sections were rinsed with TBST twice and then incubated in the SA-HRP for 30 min at room temperature (1:100 in TNB buffer; PerkinElmer), rinsed twice in TBST, and then, incubated in 3,3-DAB for 15 min at room temperature (metal-enhanced DAB, 1:10 in peroxidase substrate buffer; Thermo Fisher Scientific). Sections were rinsed in distilled water and then counterstained with Mayer's hematoxylin for 30 s. Sections were rinsed with distilled water and then dehydrated and mounted.

Plasma collection. Mice were anesthetized using a mixture of ketamine (120 mg/kg) and xylazine (20 mg/kg) using a 0.5-inch, 27-gauge needle via i.p. injection. Under anesthesia, the anterior chest wall was removed, and the left ventricle was pierced with a 0.5-inch, 20-gauge needle. Depending on the age and size of the mouse, anywhere from 300 to 900 µl of blood was slowly aspirated and dispensed, on ice, into a BD Vacutainer with K2 EDTA (lavender top) blood collection tube (367841). The blood was then processed for plasma, following the manufacturer's protocol. Plasma was stored in an Eppendorf LoBind protein microcentrifuge tube (022431102) at −80°C until use.

Measuring changes in biomarkers via ELISA. Plasma samples were thawed on ice, and a 220-µl aliquot was spun at 4°C for 20 min at 2,000 *g*. Samples were then aliquoted in 25-µl stocks. The genotypes and treatments of the samples being tested were masked to the investigator conducting the assays, and samples were randomized in the plates to prevent position effects. No samples were excluded from the analyses based on being outliers.

Measuring N3ECD with custom ELISA. N3ECD was detected in circulation using a previously described protocol (Primo et al., 2016), modified as follows. In brief, circulating N3ECD was detected with an in-house–developed, sandwich ELISA, using commercially available antibodies from R&D Systems. The capture antibody was a mAb (MAB1559; R&D Systems) that was coated on a flat-bottom Microlon 600 high-binding 96-well plate, (82050–720; VWR International) at 0.625 ng/µl in 100 µl of PBS overnight at 4°C. The recombinant human N3ECD, originally used to raise the antibodies (1559-NT-050; R&D Systems), was used as the standard, and a positive control. Samples of plasma were added at a concentration of 1:40, to 5 µl in 195 µl of reagent diluent (DY995; R&D Systems). Samples and the standard were added to the coated plate and left to incubate overnight at 4°C. For detection, we used a Bt polyclonal antibody raised against the N3ECD (BAF1559; R&D Systems) at a concentration of 0.001 mg/ml. After incubation overnight and washing, as described previously (Primo et al., 2016), an SA-HRP complex from R&D Systems (DY998), at 1× concentration from the 10× stock, was added to the plate and allowed to incubate for 40 min at room temperature. The plate was then washed five times to ensure complete removal of the SA-HRP before the subsequent steps were performed. Sulfuric acid from the ELISA reagent kit (DY008) was warmed to 37°C before the addition of 100 µl of tetramethylbenzidine provided by R&D Systems (DY008), initiating the detection phase of the reaction. After a 20-min incubation, sulfuric acid was added to terminate the reaction. The plate was then read using a SPECTRAmax plus 384 (Molecular Devices). The wavelength of the read was 450 nm. For calculating the amount of antigen present in the samples, a standard curve was plotted using Prism 6 (GraphPad Software) based on the serial diluted recombinant Notch3 protein. The OD values obtained for the samples and standards had a mean OD value for the antigen blanks subtracted from them, before being converted to a standard measurement, which we chose to represent as pg/ml.

Measuring circulating IGFBP-1. Circulating mouse IGFBP-1 was detected with an in-house–developed, sandwich ELISA using a commercially available kit (DY1588-05; R&D Systems). The capture antibody was coated on a flat-bottom Microlon 600 high-binding 96-well plate, (82050–720; VWR International) at 4 µg/ml in 100 µl/well of PBS overnight at 4°C. Samples of plasma were added at a concentration of 1:40, 5 µm in 195 µl of reagent diluent (DY995; R&D Systems). Samples and the standard were added to the coated plate and left to incubate overnight at 4°C. For the detection phase, we used the Bt polyclonal antibody raised against the mouse IGFBP-1 supplied by the kit (DY1588-05; R&D Systems) at a concentration of 400 ng/ml. The colorimetric detection reaction, termination, and plate reading were performed using the method described for the N3ECD.

Measuring circulating endostatin and HTRA1. Circulating mouse endostatin and HTRA1 were detected using commercially available, sandwich ELISA kits (MBS266186 and MBS906562, respectively; MyBiosource). Samples were analyzed, following the manufacturer's provided instructions.

Data availability. Please contact the corresponding authors for access to any data presented in this work.

Code availability. The Fiji-based script (ImageJ) designed to analyze the mural cell investment in the retinal vasculature can be made available upon request to the corresponding authors.

Online supplemental material

Fig. S1 shows image processing of vessels via the Fiji-based macro. Fig. S2 shows antibody penetration of blood–retinal barrier. Fig. S3 shows the efficiency and specificity of human Notch3 expression by the SM22 promoter-driven Cre-recombinase.

ACKNOWLEDGMENTS

The authors thank Vincent Primo, Mark Graham, Kahira Saez, and Eric Ng, for valuable discussions and advice, and Philip Seifert for expert help with TEM. The authors would like to thank the Schepens Eye Research Animal Facility, the Animal Visual Assessment Core, and the Morphology Core. The authors would especially like to thank the cureCADASIL Association for their continued interest, enthusiasm, and financial support. We thank the patients with CADASIL and their families for inspiring this work and for their support via the "CADASIL support" and the "CADASIL-ians" Facebook groups. We thank Anne McGuinness for suggesting the use of the agonist Notch3 antibody for experimentation.

We acknowledge support by cureCADASIL Association (research grant CARG2015-1 to J.F. Arboleda-Velasquez and A.A. Bigger-Allen, research alliance grants CARA2016-1 and CARA2017-1 to J.F. Arboleda-Velasquez, and summer scholarship CASS2016-1 to A.V. Sanchez), Consejo Nacional de Ciencia y Tecnología (CONACYT), México (grant 238332 to A.I. Machuca-Parra), National Institutes of Health (grants R01EY005318 to P.A. D'Amore, R00EY021624 and UH2NS100121 to J.F. Arboleda-Velasquez, and K12EY16335 and R21EY027061 to L.A. Kim), and the Department of Ophthalmology at Massachusetts Eye and Ear (to J.F. Arboleda-Velasquez). Additional support was provided by the E. Matilda Ziegler Foundation for the Blind and the Karl Kirchgessner Foundation (research grants to L.A. Kim). This work was also supported by National Institutes of Health National Eye Institute (core grant P30EY003790).

The sponsors and funding organizations had no role in the design or conduct of this research. J.F Arboleda-Velasquez is listed as an inventor in patent applications referring to the use of body fluid biomarkers in SVD and the use of Notch3 signaling manipulation for the treatment of SVD. J.F. Arboleda-Velasquez is a director and cofounder of Vastora Inc., a company with commercial interests in SVD. Genentech employs C.W. Siebel, and this employer has commercial interests in the Notch3 agonist antibody. The authors declare no additional competing financial interests.

Author contributions: P.A. D'Amore and J.F. Arboleda-Velasquez designed the project; C.W. Siebel provided materials and analyzed data; A.I. Machuca-Parra and A.A. Bigger-Allen designed the experiments and conducted in vivo work; A.I. Machuca-Parra designed the experiments and conducted in vitro work; A.V. Sanchez, A. Boutabla, J. Cardona-Vélez, and D. Amarnani conducted research; M. Saint-Geniez and L.A. Kim analyzed the data; and A.I. Machuca-Parra, A.A. Bigger-Allen, P.A. D'Amore, and J.F. Arboleda-Velasquez wrote the manuscript.

Submitted: 28 October 2016
Revised: 28 April 2017
Accepted: 8 June 2017

REFERENCES

Arboleda-Velasquez, J.F., F. Lopera, E. Lopez, M.P. Frosch, D. Sepulveda-Falla, J.E. Gutierrez, S. Vargas, M. Medina, C. Martinez De Arrieta, R.V. Lebo, et al. 2002. C455R notch3 mutation in a Colombian CADASIL kindred with early onset of stroke. *Neurology.* 59:277–279. http://dx.doi.org/10.1212/WNL.59.2.277

Arboleda-Velasquez, J.F., R. Rampal, E. Fung, D.C. Darland, M. Liu, M.C. Martinez, C.P. Donahue, M.F. Navarro-Gonzalez, P. Libby, P.A. D'Amore, et al. 2005. CADASIL mutations impair Notch3 glycosylation by Fringe. *Hum. Mol. Genet.* 14:1631–1639. http://dx.doi.org/10.1093/hmg/ddi171

Arboleda-Velasquez, J.F., Z. Zhou, H.K. Shin, A. Louvi, H.H. Kim, S.I. Savitz, J.K. Liao, S. Salomone, C. Ayata, M.A. Moskowitz, and S. Artavanis-Tsakonas. 2008. Linking Notch signaling to ischemic stroke. *Proc. Natl. Acad. Sci. USA.* 105:4856–4861. http://dx.doi.org/10.1073/pnas.0709867105

Arboleda-Velasquez, J.F., J. Manent, J.H. Lee, S. Tikka, C. Ospina, C.R. Vanderburg, M.P. Frosch, M. Rodríguez-Falcón, J. Villen, S. Gygi, et al. 2011. Hypomorphic Notch 3 alleles link Notch signaling to ischemic cerebral small-vessel disease. *Proc. Natl. Acad. Sci. USA.* 108:E128–E135. http://dx.doi.org/10.1073/pnas.1101964108

Arboleda-Velasquez, J.F., V. Primo, M. Graham, A. James, J. Manent, and P.A. D'Amore. 2014. Notch signaling functions in retinal pericyte survival. *Invest. Ophthalmol. Vis. Sci.* 55:5191–5199. http://dx.doi.org/10.1167/iovs.14-14046

Arboleda-Velasquez, J.F., C.N. Valdez, C.K. Marko, and P.A. D'Amore. 2015. From pathobiology to the targeting of pericytes for the treatment of diabetic retinopathy. *Curr. Diab. Rep.* 15:5. http://dx.doi.org/10.1007/s11892-014-0573-2

Armulik, A., G. Genové, M. Mäe, M.H. Nisancioglu, E. Wallgard, C. Niaudet, L. He, J. Norlin, P. Lindblom, K. Strittmatter, et al. 2010. Pericytes regulate the blood-brain barrier. *Nature.* 468:557–561. http://dx.doi.org/10.1038/nature09522

Baron-Menguy, C., V. Domenga-Denier, L. Ghezali, F.M. Faraci, and A. Joutel. 2017. Increased Notch3 activity mediates pathological changes in structure of cerebral arteries. *Hypertension.* 69:60–70. http://dx.doi.org/10.1161/HYPERTENSIONAHA.116.08015

Chabriat, H., A. Joutel, M. Dichgans, E. Tournier-Lasserve, and M.G. Bousser. 2009. Cadasil. *Lancet Neurol.* 8:643–653. http://dx.doi.org/10.1016/S1474-4422(09)70127-9

Choy, L., T.J. Hagenbeek, M. Solon, D. French, D. Finkle, A. Shelton, R. Venook, M.J. Brauer, and C.W. Siebel. 2017. Constitutive NOTCH3 signaling promotes the growth of basal breast cancers. *Cancer Res.* 77:1439–1452. http://dx.doi.org/10.1158/0008-5472.CAN-16-1022

Dotti, M.T., N. De Stefano, S. Bianchi, A. Malandrini, C. Battisti, E. Cardaioli, and A. Federico. 2004. A novel NOTCH3 frameshift deletion and mitochondrial abnormalities in a patient with CADASIL. *Arch. Neurol.* 61:942–945. http://dx.doi.org/10.1001/archneur.61.6.942

Erro, R., M. Moccia, M. Cervasio, S. Penco, M.B. De Caro, and P. Barone. 2015. Are granular osmiophilic material deposits an epiphenomenon in CADASIL? *Folia Neuropathol.* 53:168–171. http://dx.doi.org/10.5114/fn.2015.52414

Ghosh, M., M. Balbi, F. Hellal, M. Dichgans, U. Lindauer, and N. Plesnila. 2015. Pericytes are involved in the pathogenesis of cerebral autosomal dominant arteriopathy with subcortical infarcts and leukoencephalopathy. *Ann. Neurol.* 78:887–900. http://dx.doi.org/10.1002/ana.24512

Henshall, T.L., A. Keller, L. He, B.R. Johansson, E. Wallgard, E. Raschperger, M.A. Mäe, S. Jin, C. Betsholtz, and U. Lendahl. 2015. Notch3 is necessary for blood vessel integrity in the central nervous system. *Arterioscler. Thromb. Vasc. Biol.* 35:409–420. http://dx.doi.org/10.1161/ATVBAHA.114.304849

High, F.A., M.M. Lu, W.S. Pear, K.M. Loomes, K.H. Kaestner, and J.A. Epstein. 2008. Endothelial expression of the Notch ligand Jagged1 is required for vascular smooth muscle development. *Proc. Natl. Acad. Sci. USA.* 105:1955–1959. http://dx.doi.org/10.1073/pnas.0709663105

Holtwick, R., M. Gotthardt, B. Skryabin, M. Steinmetz, R. Potthast, B. Zetsche, R.E. Hammer, J. Herz, and M. Kuhn. 2002. Smooth muscle-

selective deletion of guanylyl cyclase-A prevents the acute but not chronic effects of ANP on blood pressure. *Proc. Natl. Acad. Sci. USA.* 99:7142–7147. http://dx.doi.org/10.1073/pnas.102650499

Jin, S., E.M. Hansson, S. Tikka, F. Lanner, C. Sahlgren, F. Farnebo, M. Baumann, H. Kalimo, and U. Lendahl. 2008. Notch signaling regulates platelet-derived growth factor receptor-beta expression in vascular smooth muscle cells. *Circ. Res.* 102:1483–1491. http://dx.doi.org/10.1161/CIRCRESAHA.107.167965

Joutel, A. 2011. Pathogenesis of CADASIL: transgenic and knock-out mice to probe function and dysfunction of the mutated gene, Notch3, in the cerebrovasculature. *BioEssays.* 33:73–80. http://dx.doi.org/10.1002/bies.201000093

Joutel, A., C. Corpechot, A. Ducros, K. Vahedi, H. Chabriat, P. Mouton, S. Alamowitch, V. Domenga, M. Cécillion, E. Marechal, et al. 1996. Notch3 mutations in CADASIL, a hereditary adult-onset condition causing stroke and dementia. *Nature.* 383:707–710. http://dx.doi.org/10.1038/383707a0

Joutel, A., M. Monet, V. Domenga, F. Riant, and E. Tournier-Lasserve. 2004. Pathogenic mutations associated with cerebral autosomal dominant arteriopathy with subcortical infarcts and leukoencephalopathy differently affect Jagged1 binding and Notch3 activity via the RBP/JK signaling Pathway. *Am. J. Hum. Genet.* 74:338–347. http://dx.doi.org/10.1086/381506

Joutel, A., M. Monet-Leprêtre, C. Gosele, C. Baron-Menguy, A. Hammes, S. Schmidt, B. Lemaire-Carrette, V. Domenga, A. Schedl, P. Lacombe, and N. Hubner. 2010. Cerebrovascular dysfunction and microcirculation rarefaction precede white matter lesions in a mouse genetic model of cerebral ischemic small vessel disease. *J. Clin. Invest.* 120:433–445. http://dx.doi.org/10.1172/JCI39733

Joutel, A., I. Haddad, J. Ratelade, and M.T. Nelson. 2016. Perturbations of the cerebrovascular matrisome: A convergent mechanism in small vessel disease of the brain? *J. Cereb. Blood Flow Metab.* 36:143–157. http://dx.doi.org/10.1038/jcbfm.2015.62

Kofler, N.M., H. Cuervo, M.K. Uh, A. Murtomäki, and J. Kitajewski. 2015. Combined deficiency of Notch1 and Notch3 causes pericyte dysfunction, models CADASIL, and results in arteriovenous malformations. *Sci. Rep.* 5:16449. http://dx.doi.org/10.1038/srep16449

Kopan, R. 2012. Notch signaling. *Cold Spring Harb. Perspect. Biol.* 4:a011213. http://dx.doi.org/10.1101/cshperspect.a011213

Li, K., Y. Li, W. Wu, W.R. Gordon, D.W. Chang, M. Lu, S. Scoggin, T. Fu, L. Vien, G. Histen, et al. 2008. Modulation of Notch signaling by antibodies specific for the extracellular negative regulatory region of NOTCH3. *J. Biol. Chem.* 283:8046–8054. http://dx.doi.org/10.1074/jbc.M800170200

Louvi, A., and S. Artavanis-Tsakonas. 2012. Notch and disease: a growing field. *Semin. Cell Dev. Biol.* 23:473–480. http://dx.doi.org/10.1016/j.semcdb.2012.02.005

Mitchell, K.J., K.I. Pinson, O.G. Kelly, J. Brennan, J. Zupicich, P. Scherz, P.A. Leighton, L.V. Goodrich, X. Lu, B.J. Avery, et al. 2001. Functional analysis of secreted and transmembrane proteins critical to mouse development. *Nat. Genet.* 28:241–249. http://dx.doi.org/10.1038/90074

Moccia, M., L. Mosca, R. Erro, M. Cervasio, R. Allocca, C. Vitale, A. Leonardi, F. Caranci, M.L. Del Basso-De Caro, P. Barone, and S. Penco. 2015. Hypomorphic NOTCH3 mutation in an Italian family with CADASIL features. *Neurobiol. Aging.* 36:547.e5–547.e11. http://dx.doi.org/10.1016/j.neurobiolaging.2014.08.021

Pippucci, T., A. Maresca, P. Magini, G. Cenacchi, V. Donadio, F. Palombo, V. Papa, A. Incensi, G. Gasparre, M.L. Valentino, et al. 2015. Homozygous NOTCH3 null mutation and impaired NOTCH3 signaling in recessive early-onset arteriopathy and cavitating leukoencephalopathy. *EMBO Mol. Med.* 7:848–858. http://dx.doi.org/10.15252/emmm.201404399

Primo, V., M. Graham, A.A. Bigger-Allen, J.M. Chick, C. Ospina, Y.T. Quiroz, J. Manent, S.P. Gygi, F. Lopera, P.A. D'Amore, and J.F. Arboleda-Velasquez. 2016. Blood biomarkers in a mouse model of CADASIL. *Brain Res.* 1644:118–126. http://dx.doi.org/10.1016/j.brainres.2016.05.008

Robinson, W., S.L. Galetta, L. McCluskey, M.S. Forman, and L.J. Balcer. 2001. Retinal findings in cerebral autosomal dominant arteriopathy with subcortical infarcts and leukoencephalopathy (cadasil). *Surv. Ophthalmol.* 45:445–448. http://dx.doi.org/10.1016/S0039-6257(00)00206-X

Roine, S., M. Harju, T.T. Kivelä, M. Pöyhönen, E. Nikoskelainen, S. Tuisku, H. Kalimo, M. Viitanen, and P.A. Summanen. 2006. Ophthalmologic findings in cerebral autosomal dominant arteriopathy with subcortical infarcts and leukoencephalopathy: a cross-sectional study. *Ophthalmology.* 113:1411–1417.e2. http://dx.doi.org/10.1016/j.ophtha.2006.03.030

Rufa, A., E. Pretegiani, P. Frezzotti, N. De Stefano, G. Cevenini, M.T. Dotti, and A. Federico. 2011. Retinal nerve fiber layer thinning in CADASIL: an optical coherence tomography and MRI study. *Cerebrovasc. Dis.* 31:77–82. http://dx.doi.org/10.1159/000321339

Rutten, J.W., E.M. Boon, M.K. Liem, J.G. Dauwerse, M.J. Pont, E. Vollebregt, A.J. Maat-Kievit, H.B. Ginjaar, P. Lakeman, S.G. van Duinen, et al. 2013. Hypomorphic NOTCH3 alleles do not cause CADASIL in humans. *Hum. Mutat.* 34:1486–1489. http://dx.doi.org/10.1002/humu.22432

Rutten, J.W., H.G. Dauwerse, G. Gravesteijn, M.J. van Belzen, J. van der Grond, J.M. Polke, M. Bernal-Quiros, and S.A. Lesnik Oberstein. 2016. Archetypal NOTCH3 mutations frequent in public exome: implications for CADASIL. *Ann. Clin. Transl. Neurol.* 3:844–853. http://dx.doi.org/10.1002/acn3.344

Soriano, P. 1999. Generalized lacZ expression with the ROSA26 Cre reporter strain. *Nat. Genet.* 21:70–71. http://dx.doi.org/10.1038/5007

Valdez, C.N., J.F. Arboleda-Velasquez, D.S. Amarnani, L.A. Kim, and P.A. D'Amore. 2014. Retinal microangiopathy in a mouse model of inducible mural cell loss. *Am. J. Pathol.* 184:2618–2626. http://dx.doi.org/10.1016/j.ajpath.2014.06.011

Wallays, G., D. Nuyens, R. Silasi-Mansat, J. Souffreau, Z. Callaerts-Vegh, A. Van Nuffelen, L. Moons, R. D'Hooge, F. Lupu, P. Carmeliet, et al. 2011. Notch3 Arg170Cys knock-in mice display pathologic and clinical features of the neurovascular disorder cerebral autosomal dominant arteriopathy with subcortical infarcts and leukoencephalopathy. *Arterioscler. Thromb. Vasc. Biol.* 31:2881–2888. http://dx.doi.org/10.1161/ATVBAHA.111.237859

Xu, X., S.H. Choi, T. Hu, K. Tiyanont, R. Habets, A.J. Groot, M. Vooijs, J.C. Aster, R. Chopra, C. Fryer, and S.C. Blacklow. 2015. Insights into autoregulation of Notch3 from structural and functional studies of its negative regulatory region. *Structure.* 23:1227–1235. http://dx.doi.org/10.1016/j.str.2015.05.001

Yoon, C.W., Y.E. Kim, S.W. Seo, C.S. Ki, S.H. Choi, J.W. Kim, and D.L. Na. 2015. NOTCH3 variants in patients with subcortical vascular cognitive impairment: a comparison with typical CADASIL patients. *Neurobiol. Aging.* 36:2443.e1–2443.e7. http://dx.doi.org/10.1016/j.neurobiolaging.2015.04.009

Zimber-Strobl, U., L.J. Strobl, C. Meitinger, R. Hinrichs, T. Sakai, T. Furukawa, T. Honjo, and G.W. Bornkamm. 1994. Epstein-Barr virus nuclear antigen 2 exerts its transactivating function through interaction with recombination signal binding protein RBP-J κ, the homologue of *Drosophila* Suppressor of Hairless. *EMBO J.* 13:4973–4982.